ELSEVIER

International Journal of Mass Spectrometry 185/186/187 (1999) 577–587

International Journal of Mass Spectrometry

Acetylacetonate (acac) anion in the gas phase: predicted structures, vibrational spectra, and photodetachment energies

Karl K. Irikura

Physical and Chemical Properties Division, National Institute of Standards and Technology, Gaithersburg, MD 20899, USA

Received 19 June 1998; accepted 18 September 1998

Abstract

The geometry and vibrational spectrum of the gas-phase acetylacetonate anion [acac$^-$; $(CH_3CO)_2CH^-$] are predicted using ab initio molecular orbital theory. At the MP2/6-31+G**//HF/6-31+G* level there are three stable conformers. In order of increasing energy, they are (**1**) a C_s structure with the carbonyl groups in an *anti* conformation, (**2**) a C_2 structure with the carbonyls pointed *exo* (about 21 kJ mol^{-1} higher than **1**), and (**3**) a C_{2v} structure with the carbonyls *endo* (about 27 kJ mol^{-1} higher than **1**). The third, least stable conformation corresponds to the geometry found in most β-diketonate coordination complexes. These three conformations are separated by barriers of about 60 kJ mol^{-1}. The infrared spectra of **1** and **2** are quite similar, but that of the *endo* structure **3** features two strong peaks instead of only one in the 1400–1700 cm^{-1} region. The enol (**4**) and di-enol (**5**) isomers are 60 kJ mol^{-1} and 230 kJ mol^{-1}, respectively, less stable than structure **1**. Vertical photodetachment of acac$^-$ can produce neutral acac in a few low-lying electronic states. At the spin-restricted B3LYP/6-31+G*//HF/6-31+G* level, the lowest vertical detachment energies are predicted to be 2.9, 2.9, 2.9, 2.1, and 1.2 eV for **1**–**5**, respectively, with an estimated uncertainty $2\sigma = 0.2$ eV. The corresponding adiabatic detachment energies (EA_0) are predicted to be 2.8, 2.8, 2.8, 2.1, and 1.2 eV. The vibrational spectra of the neutral radicals are also predicted and the vibrational structure on the photodetachment spectra is discussed. (Int J Mass Spectrom 185/186/187 (1999) 577–587)

Keywords: Ab initio; Anion; Electron affinity (EA); Vibrational spectrum; Photoelectron spectrum

1. Introduction

Acetylacetonate (diacetyl methyl anion; acac$^-$ for short) is the parent member of the β-diketonate class of chelating ligands [1,2]. Many β-diketonate complexes are volatile, and they are technologically useful for chemical vapor deposition [3]. There have been several calorimetric studies of β-diketonate complexes, but attempts to derive metal-ligand bond strengths have been frustrated by the lack of reliable thermodynamic information for the free ligands [4–6]. The most reliable data currently available appear to be the thermodynamic electron affinity, EA(acac) = 2.52 ± 0.22 eV = 243 ± 21 kJ mol^{-1}, determined by electron transfer bracketing [7], and the gas-phase acidity recommendation ΔH^0_{300}(Hacac → acac$^-$ + H^+) = 1438 ± 8 kJ mol^{-1} [8]. These quantities were combined to derive thermochemistry for the neutral acac radical [7]. The experimental studies involved speculative estimations of the spectroscopic data required for the calculation of entropies, and the authors noted that better spectroscopic

Dedicated to Professor Michael T. Bowers on the occasion of his 60th birthday.

1387-3806/99/$20.00 Published by Elsevier Science Inc.
PII S1387-3806(98)14192-1

information was needed. In particular, vibrational frequencies and barriers for methyl torsions are unknown [8], and it was assumed explicitly that $acac^-$ has only a single gas-phase structure in the 300–600 K temperature range [7]. These issues are addressed in the present study. Moreover, information relevant to the photodetachment spectroscopy of $acac^-$ is provided to encourage its measurement [9,10], which might provide a very accurate value for the electron affinity.

This article presents ab initio calculations of the structure and spectroscopy of a common ionic ligand; I should note at least a topical connection to Mike Bowers' work. Ion mobility chromatography, which was developed in his group, has proved to be a powerful and general technique for obtaining structural information about gas-phase ions [11,12]. He has made many contributions to the chemistry of transition metal ions, both with and without ligands [11,13,14]. Finally, he has a long record of using theory, ranging from the pencil-and-paper type [15] to more computationally intensive types [11–14], to enhance the value of experimental results.

2. Methods

Anion geometries for all isomers of interest were calculated at the Hartree–Fock (HF) level using 6-31+G* basis sets. Harmonic vibrational frequencies were computed analytically and scaled by a multiplicative factor of 0.8929 to predict vibrational spectra and vibrational zero-point energies (ZPEs). Relative energies of $acac^-$ isomers were computed at the frozen-core MP2 level. Polarization functions were added on the hydrogen atoms to describe hydrogen bonding better. Thus, isomerization energies were computed as $\Delta E = E$(isomer #2) $- E$(isomer #1), where E = MP2/6-31+G**//HF/6-31+G* + ZPE (scaled HF/6-31+G*). Likewise, transition states for isomerization among the keto isomers (**1**–**3**) were located on the HF/6-31+G* potential energy surface and their energies evaluated at the MP2/6-31+G** level. The transition states were characterized by vibrational analysis and verified by intrinsic-reaction coordinate calculations [16] to connect the desired structures. Approximate rate constants for isomerization were computed using transition-state theory and the rigid rotor/harmonic oscillator (RRHO) model [17]. Although the RRHO model is poor for the methyl rotations, the methyl groups are merely spectators in the isomerization reactions, so errors in their partition functions will cancel in the rate calculation. The contribution of tunneling was estimated using the Wigner approximation to be $\leq$3% at 300 K and so was neglected.

Several levels of theory were considered for computing vertical detachment energies (VDEs). Theories were tested against a set of carbon-, hydrogen-, and oxygen-containing molecules (Table 1). Since the calculated VDE is blind to the location of vibrational levels, it represents a classical approximation to the experimental VDE. Thus, for comparison with theory, the "experimental" VDE values were not always taken from the most intense peak in the anion photoelectron spectra. Instead, sometimes the three strongest peaks were fitted to a parabola to estimate the appropriate classical value for the VDE. Such interpolation was done for methyl (CH_3^-), allyl ($CH_2CHCH_2^-$), and vinoxyl (CH_2CHO^-) anions. For methoxyl anion (CH_3O^-), the vibrational origin is the strongest peak and was accepted as the VDE. Based upon the testing summarized in Table 1, spin-restricted (prefix "RO") density functional theory using the hybrid B3LYP functional [18,19] was chosen for VDE calculations on $acac^-$ isomers. Again based upon Table 1, an empirical correction of 0.07 eV was subtracted from all such VDE values and the residual (standard) uncertainty estimated conservatively as σ = 0.1 eV (1 eV = 96.485 kJ mol^{-1}). To summarize, the procedure used was VDE = ROB3LYP (radical)/6-31+G*//HF(anion)/6-31+G* − B3LYP (anion)//HF/6-31+G* − 0.07 eV ± 0.2 eV (2σ).

The procedure described above was used to compute VDEs to the lowest state of each irreducible representation of the point group of the neutral acac isomer. Other excited states cannot be computed using simple SCF methods. Instead, radical excitation energies among states of the same symmetry were computed using a multireference, first-order configu-

Table 1
Experimental vertical detachment energies (VDEs) and errors in computed VDEs obtained using the 6-31+G* basis sets and HF/6-31+G* anion geometries. Units are eV (1 eV = 96.485 kJ mol^{-1})

	C	CH_3	Allyl	O	CH_3O	Vinoxyl	RMS error	Max error
Experimental reference	1.263 [27]	0.264 [28]	0.504 [29]	1.461 [27]	1.570 [30]	1.837 [31]	—	—
				Differences between calculated and experimental values				
ROHF	−0.73	−1.43	−1.06	−1.97	−1.69	−1.04	1.39	−1.97
ROMP2	−0.29	−0.43	−0.54	−0.37	−0.15	−0.27	0.36	−0.54
ROCCSD	−0.38	−0.54	−0.65	−0.54	−0.57	−0.46	0.53	−0.65
ROCCSD(T)	−0.35	−0.47	−0.60	−0.47	−0.50	−0.40	0.47	−0.60
ROB3LYP	0.11	0.04	0.00	0.18	−0.10	0.09	0.10	0.18
ROBHandHLYP	−0.21	−0.30	−0.22	−0.35	−0.44	−0.10	0.29	−0.44
ROBLYP	0.08	0.03	−0.11	0.22	−0.17	−0.04	0.13	0.22
UHF	−0.79	−1.50	−1.73	−2.01	−1.83	−1.55	1.61	−2.01
UMP2	−0.28	−0.43	−0.22	−0.37	−0.15	0.14	0.29	−0.43
UCCSD	−0.38	−0.54	−0.68	−0.54	−0.57	−0.49	0.54	−0.68
UCCSD(T)	−0.35	−0.47	−0.59	−0.48	−0.50	−0.40	0.47	−0.59
UB3LYP	0.10	0.02	−0.11	0.16	−0.14	0.00	0.11	0.16
UBHandHLYP	−0.24	−0.33	−0.44	−0.37	−0.51	−0.29	0.38	−0.51
UBLYP	0.07	0.01	−0.16	0.26	−0.20	−0.08	0.16	0.26
OVGF [32,33]	−0.09	−0.44	−0.64	0.21	0.21	−0.35	0.37	−0.64

ration interaction method (FOCI). The reference was a state-averaged, complete-active-space self-consistent field (CASSCF) wavefunction including either the highest seven or eight occupied orbitals, CASSCF(13/7) or CASSCF(15/8). This active space includes the three occupied π orbitals and the four lone pairs on the oxygen atoms for the keto isomers and an additional valence pair for the enol and di-enol isomers. Since photodetachment from an anion is expected to excite only the electron that is removed, no virtual orbitals were included in the active space. The FOCI involves all single excitations from the CASSCF reference. In the FOCI calculations, 20 occupied and 20 virtual orbitals were frozen for keto isomers. Nineteen occupied and 19 virtual orbitals were frozen for the enol and di-enol calculations. The resulting vertical excitation energies for higher states were added to the previously computed VDEs for the lowest state to obtain VDEs to these higher states. To summarize, for states that are not the lowest of their symmetry, the procedure was VDE(state #n) = FOCI(state #n) − FOCI(state #1) + VDE(state #1). Since experimental benchmarks are scarce, no calibration study was done for this procedure. Assuming the excitation energies to be reliable to about 2000 cm^{-1}, the uncertainty for these higher VDEs was taken to be 2σ = 0.3 eV.

For selected states of the neutral radicals, adiabatic electron affinities (EA_0) were computed assuming no isomerization. Spin-restricted Hartree–Fock calculations (ROHF/6-31+G*) were used to compute radical geometries and harmonic vibrational frequencies. The vibrational frequencies were computed analytically and scaled by 0.8929. As was done for the VDEs, EA_0 values were computed at the B3LYP level and the empirical correction of −0.07 eV was applied. Thus, the procedure was EA_0 = ROB3LYP(radical)//ROHF(radical)/6-31+G* − B3LYP(anion)//HF(anion)/6-31+G* + ZPE(radical) − ZPE(anion) − 0.07 eV ± 0.2 eV (2σ). For direct comparison with (vibrationless) VDEs, vibrationless adiabatic detachment energies EA_e were computed similarly but without the ZPEs, EA_e = EA_0 − ZPE(radical) + ZPE(anion). As for the anions, relative energies of different neutral structures were computed at the ROMP2/6-31+G**//ROHF/6-31+G* level (including scaled ZPE). GAUSSIAN 94 [20] and GAMESS [21] were used for all calculations [22].

Vibrational activity in the photoelectrum spectrum was approximated by superimposing the anion geometry upon the optimized geometry of the neutral product so as to annihilate all components of their mass-weighted difference along rigid-body translation and rotation coordinates. The residual mass-weighted difference was then decomposed along the Cartesian normal modes of the neutral product. Displacements were converted to energies using the harmonic oscillator model and then converted to approximate numbers of vibrational quanta by dividing by the corresponding scaled harmonic frequencies. Large quantum numbers indicate modes that will be excited by photodetachment. This linear procedure fails for large, curved displacements, e.g. large torsional displacements for methyl groups. Thus, displacements along methyl torsions were approximately annihilated by hand prior to the projection procedure.

3. Results

The optimized geometries for the $acac^-$ anion are illustrated in Fig. 1 for the keto isomers (**1**, **2**, and **3**) and in Fig. 2 for the enol (**4**) and di-enol isomers (**5**). The symmetry point groups of the structures are C_s for **1**, C_2 for **2**, C_{2v} for **3**, C_s for **4**, and C_1 (no symmetry) for **5**. Structure **2** deviates from C_{2v} to relieve steric repulsion between the methyl groups. Similarly, structure **5** deviates from C_s to reduce repulsion between the H-acceptor hydroxyl group and the eclipsing methylene group. At the frozen-core MP2/6-31+G**//HF/6-31+G* level the respective relative energies for structures **1**–**5** are 0, 21, 27, 63, and 226 kJ mol^{-1}, including the ZPE.

Transition structures between **1** and **2** and between **1** and **3** lie 90 and 81 kJ mol^{-1} (including ZPE), respectively, above **1**. The computed barriers and entropies correspond to half-lives (at 300 K) of about 120 ms for the *exo* structure (**2** → **1**) and 0.70 ms for the *endo* structure (**3** → **1**). Only a second-order saddle point at high energy (226 kJ mol^{-1} above **2**, including ZPE) could be located along the HF/6-31+G* path of C_s symmetry connecting (idealized, C_{2v}) structures **2** and **3**. Interconversion between **2** and **3** probably occurs via **1**.

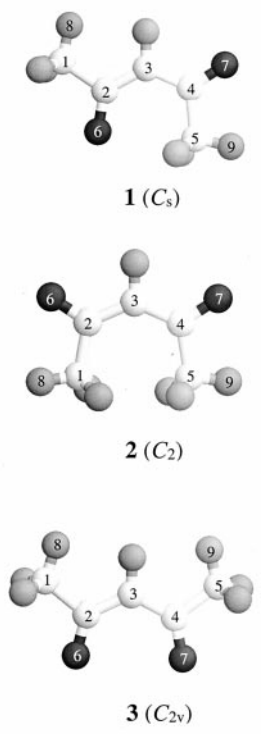

Fig. 1. Structures for the $acac^-$ anion optimized at the HF/6-31+G* level. From the top they are the *anti* (**1**), *exo* (**2**), and *endo* (**3**) conformations.

Barrier heights for soft torsions are important for

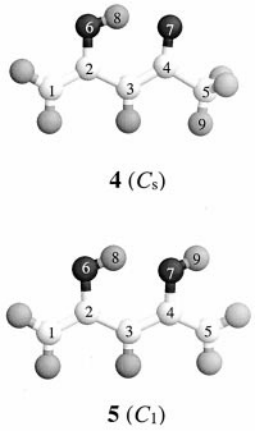

Fig. 2. Structures for the enol (**4**) and di-enol (**5**) isomers of the $acac^-$ anion, optimized at the HF/6-31+G* level.

Table 2
Scaled RHF/6-31+G* vibrational frequencies ν_i, in cm^{-1} for $acac^-$ in its *anti* (**1**), *exo* (**2**), and *endo* (**3**) geometries. Dipole intensities, in km mol^{-1}, are in parentheses

Mode	*anti* (**1**)		*exo* (**2**)		*endo* (**3**)	
i	Symm.	ν_i (*I*)	Symm.	ν_i (*I*)	Symm.	ν_i (*I*)
1	*A′*	2980 (44.2)	*A*	2980 (31.7)	A_1	2975 (53.9)
2	*A′*	2926 (45.7)	*A*	2939 (1.9)	A_1	2902 (86.6)
3	*A′*	2909 (52.5)	*A*	2911 (9.5)	A_1	2846 (14.6)
4	*A′*	2864 (44.8)	*A*	2861 (49.9)	A_1	1661 (730)
5	*A′*	2846 (54.3)	*A*	1581 (151)	A_1	1445 (19.0)
6	*A′*	1603 (264)	*A*	1461 (4.4)	A_1	1359 (6.6)
7	*A′*	1535 (1240)	*A*	1445 (6.2)	A_1	1172 (32.9)
8	*A′*	1450 (82.1)	*A*	1369 (60.6)	A_1	980 (1.0)
9	*A′*	1423 (247)	*A*	1272 (139)	A_1	892 (0.7)
10	*A′*	1415 (199)	*A*	1013 (0.6)	A_1	601 (0.1)
11	*A′*	1376 (25.2)	*A*	1006 (0.08)	A_1	335 (3.2)
12	*A′*	1358 (3.09)	*A*	738 (0.6)	A_1	163 (2.0)
13	*A′*	1256 (352)	*A*	587 (2.8)	A_2	2892 (0)
14	*A′*	1158 (40.2)	*A*	567 (8.4)	A_2	1445 (0)
15	*A′*	992 (198)	*A*	427 (9.8)	A_2	1024 (0)
16	*A′*	977 (12.3)	*A*	239 (5.1)	A_2	569 (0)
17	*A′*	927 (17.6)	*A*	122 (0.03)	A_2	89 (0)
18	*A′*	790 (1.3)	*A*	49 (0.09)	A_2	74 (0)
19	*A′*	593 (14.6)	*B*	2935 (90.9)	B_1	2892 (95.1)
20	*A′*	520 (23.4)	*B*	2918 (81.0)	B_1	1445 (3.0)
21	*A′*	383 (1.2)	*B*	2855 (7.6)	B_1	1010 (14.8)
22	*A′*	339 (0.5)	*B*	1520 (1740)	B_1	676 (18.6)
23	*A′*	193 (17.0)	*B*	1467 (12.5)	B_1	638 (68.9)
24	*A″*	2928 (26.7)	*B*	1431 (142)	B_1	158 (1.8)
25	*A″*	2890 (48.2)	*B*	1387 (149)	B_1	71 (1.6)
26	*A″*	1444 (2.7)	*B*	1345 (0.07)	B_2	2903 (30.4)
27	*A″*	1441 (3.1)	*B*	1239 (434)	B_2	2846 (83.7)
28	*A″*	1025 (0.1)	*B*	1009 (9.2)	B_2	1558 (188)
29	*A″*	1017 (10.4)	*B*	978 (154)	B_2	1450 (217)
30	*A″*	720 (76.8)	*B*	841 (57.6)	B_2	1421 (1037)
31	*A″*	622 (7.5)	*B*	756 (87.4)	B_2	1358 (8.7)
32	*A″*	558 (0.8)	*B*	562 (24.0)	B_2	1194 (199)
33	*A″*	160 (0.4)	*B*	541 (6.8)	B_2	988 (75.9)
34	*A″*	127 (1.0)	*B*	308 (25.6)	B_2	854 (30.2)
35	*A″*	98 (0.01)	*B*	203 (1.7)	B_2	490 (22.1)
36	*A″*	84 (12.0)	*B*	139 (0.2)	B_2	382 (21.7)

thermodynamic functions such as entropy [7,8]. Torsional saddle-point calculations for **1** yield classical barriers (that is, including ZPE in all modes except the torsion) of 260 and 271 cm^{-1} (3.1 and 3.2 kJ mol^{-1}), for the methyl rotors adjacent to the *endo* and *exo* carbonyls, respectively, at the MP2 level cited above. At the same level of theory, the bridging hydroxyl moiety in enol **4** has a torsional barrier of 6550 cm^{-1} (78 kJ mol^{-1}), including ZPE, at a C–C–O–H dihedral angle $\phi = 118.8°$; the most stable, hydrogen-bonded geometry has $\phi = 0$. This transition state involves some puckering and twisting of the molecule in addition to the OH torsion.

The scaled harmonic vibrational frequencies and corresponding infrared absorption intensities are summarized in Table 2 for the *anti*, *exo*, and *endo* keto conformations and in Table 3 for the enol and di-enol isomers, respectively. These vibrations may be evident as hot bands in a negative-ion photoelectron spectrum. Anions **1**–**3** have rather similar vibrational

Table 3
Scaled RHF/6-31+G* vibrational frequencies ν_i, in cm^{-1} for the enol (**4**) and di-enol (**5**) isomers of $acac^-$. Dipole intensities, in km mol^{-1}, are in parentheses

Mode	enol (**4**)		di-enol (**5**)	
i	Symm.	ν_i (*I*)	Symm.	ν_i (*I*)
1	*A′*	3309 (408)	*A*	3674 (12.6)
2	*A′*	3031 (51.9)	*A*	3637 (210)
3	*A′*	2992 (27.1)	*A*	3035 (51.4)
4	*A′*	2963 (5.3)	*A*	3023 (46.3)
5	*A′*	2901 (63.4)	*A*	2990 (16.2)
6	*A′*	2843 (72.9)	*A*	2966 (2.7)
7	*A′*	1611 (826)	*A*	2940 (12.6)
8	*A′*	1500 (660)	*A*	1568 (700)
9	*A′*	1457 (62.7)	*A*	1514 (2310)
10	*A′*	1450 (228)	*A*	1441 (11.9)
11	*A′*	1437 (311)	*A*	1408 (76.6)
12	*A′*	1367 (32.5)	*A*	1334 (335)
13	*A′*	1341 (79.2)	*A*	1308 (71.9)
14	*A′*	1246 (306)	*A*	1268 (135)
15	*A′*	1158 (34.9)	*A*	1217 (334)
16	*A′*	996 (32.0)	*A*	1154 (882)
17	*A′*	959 (47.9)	*A*	1002 (36.1)
18	*A′*	929 (46.0)	*A*	945 (60.4)
19	*A′*	873 (27.0)	*A*	890 (28.1)
20	*A′*	623 (9.4)	*A*	827 (36.8)
21	*A′*	485 (9.4)	*A*	716 (158)
22	*A′*	386 (1.6)	*A*	689 (11.1)
23	*A′*	360 (5.5)	*A*	655 (6.2)
24	*A′*	229 (16.2)	*A*	635 (6.6)
25	*A″*	2886 (48.5)	*A*	616 (50.9)
26	*A″*	1441 (1.8)	*A*	565 (139)
27	*A″*	1024 (5.2)	*A*	532 (49.5)
28	*A″*	807 (138)	*A*	491 (6.6)
29	*A″*	729 (82.0)	*A*	476 (57.5)
30	*A″*	702 (14.5)	*A*	423 (352)
31	*A″*	628 (63.0)	*A*	384 (8.2)
32	*A″*	599 (9.5)	*A*	362 (12.4)
33	*A″*	559 (38.1)	*A*	328 (224)
34	*A″*	183 (1.2)	*A*	231 (3.7)
35	*A″*	130 (2.8)	*A*	108 (3.1)
36	*A″*	103 (2.0)	*A*	82 (0.8)

spectra but do show some differences (see Table 2). The enol isomers **4** and **5** are distinguished by prominent O–H stretches at high frequency.

Table 4 summarizes some of the lower vertical detachment energies (VDEs) computed for structures **1**–**5**. The estimated uncertainty of these values is $2\sigma \approx 0.2$ eV. The geometries of selected states of the neutral radicals were computed to obtain approximate vibrationless adiabatic detachment energies, EA_e, also listed in Table 4. Including ZPE is necessary to obtain proper adiabatic electron affinities (EA_0). However, most of the ZPE corrections are small enough that $EA_0 = EA_e$ to the precision presented in Table 4. The only exception is for the $^2B_2$ state of *endo* structure **3**, for which $EA_e = 2.8 \pm 0.2$ eV and $EA_0 = 2.9 \pm 0.2$ eV. The relative energies of different structures of neutral acac were computed at the ROMP2//ROHF level to be 1.4, 16, 18, 0, and 74 kJ mol^{-1} for structures close to **1**–**5**, respectively.

Table 4
Vertical detachment energies (VDEs) and vibrationless adiabatic detachment energies (EA_e) for $acac^-$ (**1**–**5**), in eV. Estimated uncertainty is $2\sigma = 0.2$ eV except where noted otherwise. The difference VDE − EA_e may be slightly less than zero because the energies and geometries were computed using different levels of theory (R-B3LYP//RHF/6-31+G*)

Structure	Final state	VDE (eV)	EA_e (eV)	Diff (eV)
1	$^2A''$	2.9	2.8	0.11
1	$1\ ^2A'$	3.6	3.6	−0.01
1	$2\ ^2A'$	4.0 ± 0.3		
2	$1\ ^2B$	2.9	2.8	0.09
2	^2A	4.2		
2	$2\ ^2B$	4.5 ± 0.3		
3	$^2B_{(1)}$	2.9	2.8	0.15
3	$^2B_2$	3.2	2.8	0.40
3	$^2A_1$	4.0		
3	$^2A_2$	6.4		
4	$1\ ^2A''$	2.1	2.1	0.06
4	$^2A'$	3.9		
4	$2\ ^2A''$	4.5 ± 0.3		
5	$1\ ^2A$	1.2	1.2	0.05
5	$2\ ^2A$	3.6 ± 0.3		
5	$3\ ^2A$	5.2 ± 0.3		

Qualitative predictions of vibrational activity may be obtained by comparing anion and neutral geometries; selected geometric parameters are listed in Table 5. Quantitative predictions are usually based upon vibrational Franck–Condon calculations. However, calculating 36-dimensional Franck–Condon factors is beyond the scope of this study. Instead, the simple procedure described in the Methods section can be used to predict which vibrational modes will be most strongly excited by the photodetachment process. Scaled vibrational frequencies for neutral acac radicals are collected in Table 6. For structure **1**, detachment to the $^2A''$ state will cause most excitation of

Table 5
Selected geometric parameters for isomers (**1**–**5**) of anionic and neutral acac (neutral values italicized and in parentheses). Geometries were optimized at the spin-restricted HF/6-31+G* level. Bond lengths are in Å (1 Å = 10^{-10} m) and angles are in degrees

Bond lengths (Å)	**1**	**2**	**3**	**4**	**5**
C(1) C(2)	1.531 (*1.511*)	1.533 (*1.512*)	1.537 (*1.512*)	1.350 (*1.441*)	1.357 (*1.339*)
C(2) C(3)	1.406 (*1.479*)	1.418 (*1.484*)	1.422 (*1.487*)	1.455 (*1.359*)	1.436 (*1.443*)
C(2) O(6)	1.237 (*1.198*)	1.233 (*1.198*)	1.222 (*1.193*)	1.348 (*1.322*)	1.363 (*1.350*)
C(3) C(4)	1.429 (*1.488*)	1.418 (*1.484*)	1.422 (*1.487*)	1.379 (*1.457*)	1.396 (*1.442*)
C(4) C(5)	1.523 (*1.507*)	1.533 (*1.512*)	1.537 (*1.512*)	1.522 (*1.510*)	1.376 (*1.335*)
C(4) O(7)	1.229 (*1.199*)	1.233 (*1.198*)	1.222 (*1.193*)	1.264 (*1.215*)	1.390 (*1.363*)
Bond angles (degree)	**1**	**2**	**3**	**4**	**5**
C(1) C(2) C(3)	116.3 (*116.0*)	122.8 (*122.2*)	115.5 (*116.1*)	125.0 (*122.4*)	125.0 (*120.3*)
C(1) C(2) O(6)	115.5 (*122.0*)	114.8 (*120.5*)	115.7 (*122.3*)	118.5 (*113.9*)	115.9 (*118.7*)
C(2) C(3) C(4)	127.1 (*127.5*)	132.7 (*132.2*)	127.5 (*123.7*)	123.7 (*122.2*)	129.2 (*128.8*)
C(3) C(4) C(5)	119.7 (*121.3*)	122.8 (*122.2*)	115.5 (*116.1*)	118.4 (*117.4*)	128.6 (*123.0*)
C(3) C(4) O(7)	122.7 (*117.0*)	122.4 (*117.3*)	128.8 (*121.6*)	126.1 (*122.1*)	115.8 (*114.7*)
Dihedral angles (degree)	**1**	**2**	**3**	**4**	
C(1) C(2) C(3) C(4)	180 (*180*)	1.9 (*12.5*)	180 (*154.1*)		
C(2) C(3) C(4) C(5)	0 (*0*)	1.9 (*12.5*)	180 (*154.1*)		
C(3) C(2) C(1) H(8)	0 (*180*)	167.8 (*171.2*)	0 (*178.6*)		
C(3) C(4) C(5) H(9)	180 (*180*)	167.8 (*171.2*)	0 (*178.6*)	0 (*180*)	

modes 19, 22, and 14 (Table 6). Detachment to the $^2A'$ state will excite principally modes 7 and 14. Detachment from structure **2** leads to strongest excitation of modes 18, 16, and 12 of the radical. The photoelectron spectrum of the canonical structure **3** to the ground ^2B state of the radical, which is distorted to the C_2 point group, is expected to show most vibrational activity in modes 18, 13, and 11, in that order. If the excited $^2B_2$ state of the radical is formed instead, it will be vibrationally excited mostly in modes 12 and 11 and more weakly in mode 10. Detachment from the enol structure **4** causes most excitation in vibrations 8 and 15. For the di-enol structure **5**, the longest vibrational progressions are expected in the few modes at lowest frequency, and possibly in the highest-frequency mode also. These results are summarized in Table 7.

4. Discussion

Different isomers of neutral or anionic acac (**1**–**5**) do not appear to have been discussed previously in the literature. The present MP2//HF calculations indicate that the most stable structure for free $acac^-$ in the gas phase is *anti* (**1**) and not the canonical coordinating structure **3**. Although there is evidence for the *anti* conformation in coordination chemistry, structure **3** predominates heavily [2]. These results are consistent with previous studies of related compounds. Different conformers of the homologous neutral radical $HC(CHO)_2$, derived from malonaldehyde instead of acetylacetone, have been studied using Hartree–Fock theory [23]. Three stable structures of C_s symmetry were found, with two close-lying electronic states for each structure. The formyl torsions in the homolog $EtC(CHO)_2$ were considered in an earlier study, although only a single structure was presented [24].

The conformational preference for structure **1** is probably driven by repulsion between the *endo* moieties, which may be either methyl groups (steric crowding) or negatively charged oxygen atoms (electrostatic repulsion). The *endo* moieties in structure **1** are different, which minimizes both repulsive interactions. Structure **2** has slightly more favorable electrostatics than **1** but much worse sterics. Structure **3** suffers from a small O–O distance. As a result of the greater *endo* repulsion, the sum of the three central (*endo*) bond angles is larger for the less stable

Table 6
Harmonic vibrational frequencies for neutral acac radicals computed at the ROHF/6-31+G* level and scaled by 0.8929

Mode	Anti, $^2A''$	Anti, $^2A'$	Exo, ^2B	Endo, ^2B	Endo, $^2B_2$	Enol	Di-enol
1	3025 (a')	3003 (a')	3038 (a)	3005 (a)	3064 (a_1)	3427 (a')	3674 (a)
2	2970 (a')	2966 (a')	2972 (a)	2968 (a)	2959 (a_1)	3113 (a')	3657 (a)
3	2969 (a')	2961 (a')	2930 (a)	2911 (a)	2880 (a_1)	3028 (a')	3082 (a)
4	2886 (a')	2890 (a')	2882 (a)	2862 (a)	1556 (a_1)	3010 (a')	3071 (a)
5	2865 (a')	2863 (a')	1744 (a)	1786 (a)	1441 (a_1)	2967 (a')	3047 (a)
6	1749 (a')	1735 (a')	1451 (a)	1441 (a)	1385 (a_1)	2866 (a')	3000 (a)
7	1738 (a')	1576 (a')	1441 (a)	1434 (a)	1298 (a_1)	1689 (a')	2986 (a)
8	1434 (a')	1444 (a')	1389 (a)	1382 (a)	1011 (a_1)	1563 (a')	1591 (a)
9	1426 (a')	1435 (a')	1239 (a)	1185 (a)	968 (a_1)	1435 (a')	1563 (a)
10	1393 (a')	1388 (a')	1023 (a)	1029 (a)	621 (a_1)	1432 (a')	1434 (a)
11	1390 (a')	1381 (a')	1000 (a)	963 (a)	423 (a_1)	1414 (a')	1403 (a)
12	1356 (a')	1334 (a')	735 (a)	812 (a)	241 (a_1)	1378 (a')	1352 (a)
13	1230 (a')	1257 (a')	546 (a)	615 (a)	2941 (a_2)	1344 (a')	1330 (a)
14	1158 (a')	1151 (a')	499 (a)	500 (a)	1442 (a_2)	1198 (a')	1300 (a)
15	1012 (a')	982 (a')	392 (a)	302 (a)	1042 (a_2)	1157 (a')	1196 (a)
16	945 (a')	955 (a')	204 (a)	155 (a)	561 (a_2)	990 (a')	1161 (a)
17	904 (a')	914 (a')	135 (a)	106 (a)	174 (a_2)	971 (a')	981 (a)
18	765 (a')	800 (a')	29 (a)	42 (a)	82 (a_2)	903 (a')	958 (a)
19	597 (a')	603 (a')	2970 (b)	2968 (b)	2941 (b_1)	891 (a')	917 (a)
20	511 (a')	440 (a')	2938 (b)	2911 (b)	1442 (b_1)	631 (a')	859 (a)
21	358 (a')	369 (a')	2874 (b)	2862 (b)	1036 (b_1)	485 (a')	841 (a)
22	305 (a')	316 (a')	1732 (b)	1747 (b)	719 (b_1)	369 (a')	817 (a)
23	179 (a')	183 (a')	1455 (b)	1443 (b)	657 (b_1)	347 (a')	683 (a)
24	2945 (a'')	2973 (a'')	1428 (b)	1435 (b)	159 (b_1)	212 (a')	679 (a)
25	2915 (a'')	2912 (a'')	1383 (b)	1399 (b)	79 (b_1)	2915 (a'')	671 (a)
26	1441 (a'')	1444 (a'')	1310 (b)	1366 (b)	2960 (b_2)	1443 (a'')	614 (a)
27	1439 (a'')	1440 (a'')	1221 (b)	1142 (b)	2880 (b_2)	1031 (a'')	556 (a)
28	1021 (a'')	1035 (a'')	1018 (b)	1012 (b)	1698 (b_2)	780 (a'')	534 (a)
29	1008 (a'')	1022 (a'')	980 (b)	959 (b)	1486 (b_2)	763 (a'')	482 (a)
30	656 (a'')	810 (a'')	849 (b)	852 (b)	1433 (b_2)	662 (a'')	431 (a)
31	514 (a'')	580 (a'')	660 (b)	605 (b)	1378 (b_2)	576 (a'')	366 (a)
32	474 (a'')	513 (a'')	552 (b)	497 (b)	1146 (b_2)	523 (a'')	353 (a)
33	165 (a'')	161 (a'')	463 (b)	421 (b)	996 (b_2)	333 (a'')	310 (a)
34	109 (a'')	108 (a'')	294 (b)	341 (b)	882 (b_2)	164 (a'')	224 (a)
35	89 (a'')	95 (a'')	202 (b)	105 (b)	526 (b_2)	110 (a'')	109 (a)
36	35 (a'')	43 (a'')	88 (b)	52 (b)	391 (b_2)	63 (a'')	61 (a)

isomers: 375° (**1**), 378° (**2**), and 385° (**3**). For the neutral acac radical, the relative stabilities are the same as for the anion except that the enol structure (**4**) is favored over the *anti* form (**1**) by a small margin (1.4 kJ mol^{-1}). Neutralization stabilizes the enol and di-enol isomers by 64 and 153 kJ mol^{-1}, respectively, relative to structure **1**. Enolization is probably more unfavorable for the anions because it forces negative charge from oxygen atoms onto carbon atoms that are less electronegative. Indeed, the sum of the HF/6-31+G* Mulliken populations on the carbons, including attached hydrogens, is approximately −0.3, −0.5, and −0.9 in anions **1**, **4**, and **5**, respectively, compared with values of −0.2, −0.01, and +0.1 in the corresponding neutral radicals.

The methyl torsion barriers in **1** are computed at the MP2//HF level to be about 3.1 kJ mol^{-1}. The contributions to entropy and enthalpy can be estimated using the computed geometry of **1** and strongly approximating the torsional potential as proportional to cos (3θ) [25]. The resulting contributions are S°_{300} = 12.9 J mol^{-1} K, and H°_{300} = 1.6 kJ mol^{-1} for each methyl rotor. In contrast, scaled Hartree–Fock harmonic frequencies lead to harmonic-oscilla-

Table 7
Principal vibrational modes that are excited upon photodetachment. Modes are ordered by decreasing excitation. Scaled HF/6-31+G* frequencies are in cm^{-1} (1 cm^{-1} = 0.01196 kJ mol^{-1})

Isomer	State	Mode	Freq (cm^{-1})	Assignment
1	$^2A''$	34	109	Methyl torsion
		19	597	Methyl C–C stretch
		22	305	C–C(O)–C bend
		14	1158	CH bend/C–C stretch
1	$^2A'$	34 + 35	108 + 95	Methyl torsion (sym + antisym)
		7	1576	Methyl C–C stretch
2	^2B	18	28	Acyl torsion
		16	204	Bend (CH_3 . . . CH_3 "stretch")
3	$^2B_{(1)}$	17	106	Methyl torsion (sym)
		18	42	Acyl torsion
		13	615	Methyl C–C stretch
3	$^2B_2$	12	241	C–C(O)–C bend
		11	423	Bend (O . . . O "stretch")
		10	621	C–C stretch/bend (O . . . O "stretch")
4	$^2A''$	36	63	Methyl torsion
		8	1563	C–O–H bend/C–C(OH) stretch
		15	1157	Methyne rock/C═CH_2 stretch

tor values of S°_{300} = 14.7 and 12.6 J mol^{-1} K and H°_{300} = 8.2 and 8.1 kJ mol^{-1} for the two methyl oscillators. Similar results are expected for methyl rotors in the other anionic structures.

The likely precursor molecule 2,4-pentanedione (acetylacetone; Hacac) exists in the gas phase as an equilibrium mixture of keto and enol isomers, with the enol form predominating [6,26]. Thus, gas-phase proton abstraction from Hacac by a strong base may kinetically produce enol **4** instead of the more stable keto isomers. Structure **4** may be distinguished from **1**–**3** by its lower detachment energy and by its vibrational spectrum (Table 2). Structure **5** is unlikely to be found, since it is much less stable than its isomers and is not an obvious product from reaction of Hacac with a base.

Choosing a value for EA(acac) from Table 4 is more problematic than usual. The most stable conformation of the anion is *anti* (**1**), so for the cold, equilibrated anion the adiabatic detachment energy is that of **1**, 2.8 ± 0.2 eV (2σ). Starting from neutral acac, however, the relative ROMP2/6-31+G**//ROHF/6-31+G* energies (including ZPE) are 1.4, 16, 18, 0, and 74 kJ mol^{-1} for structures close to **1**–**5**, respectively. Thus, an enol structure close to **4** may predominate in a cold population of radicals; the corresponding adiabatic electron affinity is 2.1 ± 0.2 eV (2σ). An experimental value, EA(acac) = 2.52 ± 0.22 eV, was obtained by charge-transfer bracketing [7]. In that experiment, $acac^-$ was generated by dissociative electron attachment to gaseous $Co(acac)_3$ and thermalized by about 30 collisions with a bath gas of cyclohexane. Charge transfer to reagents of established electron affinity serves to bracket $\Delta_{detachment}G$(acac) at the temperature of the experiment. Because the temperature is probably 300 K or greater (RT ≈ 2.5 kJ mol^{-1}), the product acac radicals are a mixture of *anti* and enol structures. In addition, the lowest vibrational frequencies in neutral acac (30–60 cm^{-1}) are lower than those in the anion (50–100 cm^{-1}). Thus, the entropy for detachment from $acac^-$ may be unusually large, resulting in an underestimated value for EA ≈ $\Delta_{detachment}H = \Delta_{detachment}G + T\Delta_{detachment}S$. The theoretical value of 2.8 ± 0.2 eV (2σ) may be preferable for the thermodynamic electron affinity.

For each structure, the lowest-energy ionization is from the π molecular orbital expected from a pentadienyl-type anion. This is a nonbonding orbital with most of its amplitude on the central carbon and on atoms 1 and 5 in the π chain. Ionizations at higher

energy (but less than 5 eV) are from lone pairs on the carbonyl oxygen atoms.

The difference between the vertical and adiabatic detachment energies (Table 4) represents the expected energy difference between the strongest peak in the photoelectron spectrum and the corresponding spectroscopic origin. When this difference is large, small Franck–Condon factors are expected near the band origin and it may be too weak to be observed. For $acac^-$, the largest difference between vertical and adiabatic detachment energies is for detachment from the *endo* anion to the $^2B_2$ state of the radical. The electron is removed from the b_2 combination of the oxygen lone pairs that is antibonding between the oxygen atoms. Thus, the $^2B_2$ state has net bonding between the oxygens, and the O–O distance decreases dramatically from 3.08 Å to 2.03 Å upon electron detachment.

5. Conclusions

Four isomers of the $acac^-$ anion (**1**–**4**) are probably accessible by gas-phase deprotonation of acetylacetone. The present calculations indicate that the adiabatic detachment energy of $acac^-$ anion is $DE_0 = 2.8 \pm 0.2$ eV (2σ), somewhat higher, but possibly more accurate, than the value EA = 2.52 ± 0.22 eV obtained by experimental charge-transfer bracketing [7]. Although all conformations of acac radical have low-lying excited states, only the *endo* conformation (**3**) has two states within 3 eV (adiabatic) of the corresponding anion.

Geometric relaxation following photodetachment is probably mild enough for band origins to be observed in the photoelectron spectrum of $acac^-$. However, the relative energies of conformational isomers and tautomers are different for the anion and for the neutral radical, so the apparent adiabatic electron affinity of the neutral radical may be 2.1 ± 0.2 eV (2σ), which is lower than the adiabatic detachment energy for the anion. This unusual situation results from the chemical heterogeneity of any equilibrated population of neutral or anionic "acac." The actual thermodynamic electron affinity that connects anion **1** with a radical with a structure like **4** (or possibly **1**), is predicted to be $EA_0 = 2.8 \pm 0.2$ eV (2σ).

References

[1] F.A. Cotton, G. Wilkinson, Advanced Inorganic Chemistry: A Comprehensive Text, 4th ed., Wiley, New York, 1980.
[2] K. Nakamoto, Infrared and Raman Spectra of Inorganic and Coordination Compounds, 5th ed., Vol. B, Wiley, New York, 1997.
[3] Chemical Vapor Deposition: Principles and Applications, M.L. Hitchman, K.F. Jensen (Eds.), Academic, London, 1993.
[4] E. Giera, W. Kakolowicz, J. Rozniatowska, Thermochim. Acta 210 (1992) 41.
[5] E.H. Jamea, G. Pilcher, Thermochim. Acta 97 (1986) 77.
[6] K.J. Cavell, G. Pilcher, J. Chem. Soc., Faraday Trans. 1 73 (1977) 1590.
[7] P. Sharpe, D.E. Richardson, J. Am. Chem. Soc. 113 (1991) 8339.
[8] J.B. Cumming, P. Kebarle, Can. J. Chem. 56 (1978) 1.
[9] P.G. Wenthold, J.B. Kim, W.C. Lineberger, J. Am. Chem. Soc. 119 (1997) 1354.
[10] P.G. Wenthold, W.C. Lineberger, J. Am. Chem. Soc. 119 (1997) 7772.
[11] P. Weis, P.R. Kemper, M.T. Bowers, J. Phys. Chem. A 101 (1997) 8207.
[12] S. Lee, T. Wyttenbach, M.T. Bowers, Int. J. Mass Spectrom. Ion Processes 167 (1997) 605.
[13] J.E. Bushnell, P. Maître, P.R. Kemper, M.T. Bowers, J. Chem. Phys. 106 (1997) 10 153.
[14] J. Gidden, P.A.M. van Koppen, M.T. Bowers, J. Am. Chem. Soc. 119 (1997) 3935.
[15] T. Su, M.T. Bowers, Int. J. Mass Spectrom. Ion Phys. 12 (1973) 347.
[16] C. Gonzalez, H.B. Schlegel, J. Phys. Chem. 94 (1990) 5523.
[17] K.K. Irikura, "Essential statistical thermodynamics," in Computational Thermochemistry: Prediction and Estimation of Molecular Thermodynamics, ACS Symposium Series 677, K.K. Irikura, D.J. Frurip (Eds.), Washington, DC, American Chemical Society, 1998, p. 402.
[18] A.D. Becke, J. Chem. Phys. 98 (1993) 5648.
[19] P.J. Stephens, F.J. Devlin, C.F. Chabalowski, M.J. Frisch, J. Phys. Chem. 98 (1994) 11 623.
[20] M.J. Frisch, G.W. Trucks, H.B. Schlegel, P.M.W. Gill, B.G. Johnson, M.A. Robb, J.R. Cheeseman, T. Keith, G.A. Petersson, J.A. Montgomery, K. Raghavachari, M.A. Al-Laham, V.G. Zakrzewski, J.V. Ortiz, J.B. Foresman, J. Cioslowski, B.B. Stefanov, A. Nanayakkara, M. Challacombe, C.Y. Peng, P.Y. Ayala, W. Chen, M.W. Wong, J.L. Andres, E.S. Replogle, R. Gomperts, R.L. Martin, D.J. Fox, J.S. Binkley, D.J. Defrees, J. Baker, J.P. Stewart, M. Head-Gordon, C. González, J.A. Pople, GAUSSIAN 94, Gaussian, Inc., Pittsburgh, PA, 1995.
[21] M.W. Schmidt, K.K. Baldridge, J.A. Boatz, S.T. Elbert, M.S. Gordon, J.H. Jensen, S. Koseki, N. Matsunaga, K.A. Nguyen,

S.J. Su, T.L. Windus, M. Dupuis, J.A. Montgomery, J. Comput. Chem. 14 (1993) 1347.
[22] Certain commercial materials and equipment are identified in this article in order to specify procedures completely. In no case does such identification imply recommendation or endorsement by the National Institute of Standards and Technology, nor does it imply that the material or equipment identified is necessarily the best available for the purpose.
[23] S. Di Bella, G. Lanza, I.L. Fragalà, J. Chem. Soc., Faraday Trans. 91 (1995) 2709.
[24] J. Espinosa-Garcia, F.J. Olivares del Valle, G. Leroy, M. Sana, J. Mol. Struct. 258 (1992) 315.
[25] K.S. Pitzer, W.D. Gwinn, J. Chem. Phys. 10 (1942) 428.
[26] G. Buemi, C. Gandolfo, J. Chem. Soc., Faraday Trans. 2 85 (1989) 215.
[27] S.G. Lias, J.E. Bartmess, J.F. Liebman, J.L. Holmes, R.D. Levin, W.G. Mallard, J. Phys. Chem. Ref. Data 17 (1988) Suppl. 1.
[28] G.B. Ellison, P.C. Engelking, W.C. Lineberger, J. Am. Chem. Soc. 100 (1978) 2556.
[29] P.G. Wenthold, M.L. Polak, W.C. Lineberger, J. Phys. Chem. 100 (1996) 6920.
[30] P.C. Engelking, G.B. Ellison, W.C. Lineberger, J. Chem. Phys. 69 (1978) 1826.
[31] G.B. Ellison, P.C. Engelking, W.C. Lineberger, J. Phys. Chem. 86 (1982) 4873.
[32] W. von Niessen, J. Schirmer, L.S. Cederbaum, Comput. Phys. Rep. 1 (1984) 57.
[33] V.G. Zakrzewski, J.V. Ortiz, J. Phys. Chem. 100 (1996) 13 979.